Rare Metal Materials and Engineering
Volume 54, Issue 9, September 2025
Available online at www.rmme.ac.cn

Science Press

Cite this article as: Guo Zilong, Li Zhaoxi, Guo Wei, et al. Microstructure and Mechanical Properties of Transient Liquid-Phase Diffusion Bonded GH5188 Joint Added with BNi-5 Interlayer[J]. Rare Metal Materials and Engineering, 2025, 54(09): 2177-2188. DOI: https://doi.org/10.12442/j.issn.1002-185X.20240452.

ARTICLE

Microstructure and Mechanical Properties of Transient Liquid-Phase Diffusion Bonded GH5188 Joint Added with BNi-5 Interlayer

Guo Zilong[1,2], Li Zhaoxi[1,2], Guo Wei[1], Liu Pengkun[1,2], Li Jinglong[1], Xiong Jiangtao[2]

[1] State Key Laboratory of Solidification Processing, Northwestern Polytechnical University, Xi'an 710072, China; [2] Shaanxi Key Laboratory of Friction Welding Technologies, Northwestern Polytechnical University, Xi'an 710072, China

Abstract: The transient liquid-phase (TLP) diffusion bonding of GH5188 with a BNi-5 interlayer was focused on. Parameters were chosen and optimized for GH5188 alloy according to the TLP joining mechanism. The microstructure evolution and mechanical properties of the joints were studied. Results show that the relatively complete isothermal solidification zone (ISZ) ensures a reliable connection of the base metal (BM). Within the temperature range of 1110–1190 °C, higher bonding temperatures can widen ISZ and promote joint composition homogenization, thus improving mechanical properties. However, the increase in precipitated phase has an adverse effect on the mechanical properties of the joint. The maximum shear strength, reaching 482 MPa, is achieved at 1130 °C, representing 84.6% of BM strength. Within the pressure range of 5–15 MPa, both precipitated phases in adiabatic solidification zone (ASZ) and voids generated by partial melting increase. On the contrary, their sizes decrease significantly under higher bonding pressure, resulting in an upward trend in alloy mechanical properties. The maximum shear strength of 490 MPa is attained at a bonding pressure of 15 MPa. The joint exhibits a typical mixed fracture pattern, with the small brittle $M_{23}C_6$ phase and voids significantly impacting mechanical properties. Nano-indentation tests indicate that ASZ is a potential source of cracks.

Key words: TLP diffusion bonding; GH5188 cobalt-based superalloy; BNi-5 interlayer; microstructure evolution; mechanical property

1 Introduction

Cobalt-based superalloys exhibit exceptional properties, including superior creep resistance, corrosion resistance, thermal fatigue resistance, and high-temperature strength[1–3]. These alloys use Co as the matrix element and incorporate significant amounts of Ni, Cr, and W, along with smaller quantities of Mo, La, Ti, and others. Compared to nickel-based superalloys, cobalt-based superalloys offer higher thermal conductivity and a lower thermal expansion coefficient, making them essential for applications requiring thermal fatigue resistance[4–6]. GH5188, a specific cobalt-based superalloy, exhibits exceptional corrosion resistance, thermal fatigue resistance, and mechanical properties at elevated temperatures. As a key material employed in the fabrication of gas turbine components, such as combustion chamber walls, outer walls, seals, and exhaust nozzles[7–12], GH5188 plays a crucial role in advanced manufacturing fields. Therefore, the development of a reliable and effective bonding method for this material significantly influences its application in these vital and cutting-edge areas.

Transient liquid phase (TLP) bonding combines the advantages of diffusion bonding and brazing, consequently becoming a promising method for bonding GH5188. This approach enhances the applicability of alloy in crucial advanced fields[13–17]. Wei et al[18] investigated the microstructure and mechanical properties of GH5188 through selective laser melting, and revealed that the superior

Received date: October 24, 2024
Foundation item: National Natural Science Foundation of China (52075449, 5197052086)
Corresponding author: Li Jinglong, Ph. D., Professor, State Key Laboratory of Solidification Processing, Northwestern Polytechnical University, Xi'an 710072, P. R. China, E-mail: lijinglg@nwpu.edu.cn;Guo Wei, Ph. D., Professor, State Key Laboratory of Solidification Processing, Northwestern Polytechnical University, Xi'an 710072, P. R. China, E-mail: nwpuweiguo@nwpu.edu.cn

elongation of the joint was attributed to the presence of fine, non-brittle carbides, preventing premature fracture and enhancing ductility before necking. Additionally, the study of Pouranvari et al[19] on the TLP bonding of the Ni-based IN718 superalloy highlighted the significant influence of solidification (including isothermal and non-isothermal processes) on bonding time. The distribution of the eutectic structure played a crucial role in determining the mechanical properties of the joint. Under the eutectic-free conditions, in which isothermal solidification was completed, the shear strength of the joints was controlled by the hardness of the isothermal solidification zone (ISZ), which was influenced by bonding temperature. Through proper design of process parameters, TLP diffusion bonding can obtain joints with comparable tensile shear strength to the base metal (BM) [19–26]. Although extensive research has been conducted on TLP diffusion bonding of nickel-based superalloys, there are still few reports on TLP diffusion bonding of GH5188 alloy. It is unclear how TLP process parameters affect the interfacial properties, microstructure evolution, and mechanical properties of the GH5188 joint. Therefore, conducting an in-depth study of TLP diffusion bonding technique for GH5188 alloy holds great significance in advancing its engineering applications.

This study focuses on TLP diffusion bonding of GH5188 with a BNi-5 interlayer. Multiple parameters were used taking the features of GH5188 alloy's component and TLP joining mechanism into consideration. The microstructure of the typical interface and mechanical properties of the joint were evaluated. The parameters optimization, microstructure evolution, formation mechanism, mechanical properties, and strengthening mechanism of TLP diffusion bonded joint were discussed comprehensively.

2 Experiment

BM was hot-rolled GH5188 sheet, with a tensile strength of 950 MPa and a shear strength of 570 MPa. The specific composition is shown in Table 1. The BNi-5 filler alloy was chosen as the interlayer, whose melting point is 1080–1135 °C with a specific composition shown in Table 2. The brazing material was mixed with an organic binder and coated on the surface to be bonded with a thickness of 50 μm. Before the bonding, GH5188 sheet was cut to the desired size of 50 mm× 25 mm using a wire cutter, and then polished step by step with sandpapers of 80#, 160#, 240#, 600#, 1000#, 1200#, 1500#, and 2000# and a grinding paste (2.5 μm) to obtain a mirror finish. Then, the sample was put into an acid solution for acid pickling, wiped with alcohol and blown dried with cold air. The joint was assembled, as shown in Fig.1, and the upper and lower pressures came from the graphite compression heads. Mica sheets were used as the barrier layers between the samples, the compression heads, and the gaskets. The diffusion bonding equipment used for the test was the radiation heating bonding machine. The metallographic morphology of the joints' interfaces was observed by scanning electron microscope (SEM, ZEISS Sigma 300), and the elements in the bonding zone and precipitated phases were analyzed by the electron probe micro-analysis (EPMA) with the electron probe (JXA-8530F Plus). The shearing tests were conducted using the Instron-3382 universal testing machine. The morphologies of the joint fracture interface and the longitudinal section were observed by SEM (Helios G4 CX) to analyze the fracture behavior of the joints.

To accelerate the interdiffusion between the interlayer and BM, the bonding temperature should be elevated. However, to prevent the abnormal grain growth caused by the elimination of pinning effect, the bonding temperature must be kept below the solid solution temperature of $M_{23}C_6$. Therefore, the optimal bonding temperature range is 1110 °C to 1190 °C, with a 20 °C interval. Considering the yield condition and small deformation requirements at high temperatures, a reasonable range of pressure and bonding time should be selected. Finally, the pressure was selected to be 5, 10, 15 MPa, and the bonding time was set to be 30 and 60 min. For the post-bonding heat treatment, the temperature was chosen to be 1000 °C and the required time is referred as the bonding time. This stage was designed for the diffusion between BM and interlayer.

3 Results and Discussion

3.1 Typical joint microstructure

Fig. 2 illuminates the microstructure of the bond achieved under conditions of 1130 °C, bonding pressure 10 MPa, and homogenization for 1 h. The bonding interface is distinctly divided into four regions: zone 1, 2, 3, and 4, representing the adiabatic solidification zone (ASZ), ISZ, diffusion-affected zone (DAZ), and BM, respectively. Notably, there is an absence of large-scale continuous eutectic structure resulting from non-isothermal solidification (Fig. 2a). Additionally, the BNi-5 solder alloy, containing a relatively high content of Si, readily forms silicide with Cr, Co, and W.

The distribution of precipitated phases in the four regions shows significant variations. ASZ has a small amount of large gray phase A and white phase B surrounded by phase A. ISZ exhibits a uniform microstructure with a small amount of gray phase C. DAZ contains numerous white strip phase D, while BM area has a small amount of white precipitate (E). To ascertain the composition of these precipitated phases, an energy dispersive X-ray electroscope (EDS) analysis was conducted on the bond zone (Fig. 3). The analysis reveals that the Ni content in the joint weld zone is higher than that in BM, while the contents of Co, W, and Si are lower (Fig. 3). Specifically, the matrix in BM area is identified as γ-Co,

Table 1 Chemical composition of GH5188 sheet (wt%)

C	Si	Ni	Cr	W	La	Fe	Ni	Co
0.05–0.15	0.20–0.50	20–24	20–24	13–16	0.03–0.12	≤3.00	≤1.25	Bal.

Table 2 Chemical composition of BNi-5 brazing material (wt%)

Cr	Si	Co	Ni
18.50–19.50	9.75–10.50	0.10	Bal.

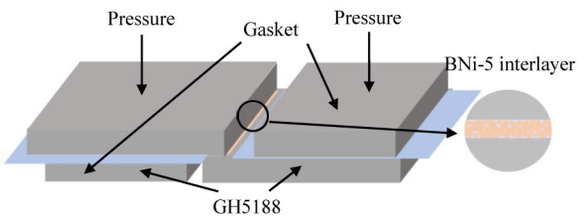

Fig.1 Bonding assembly schematic diagram

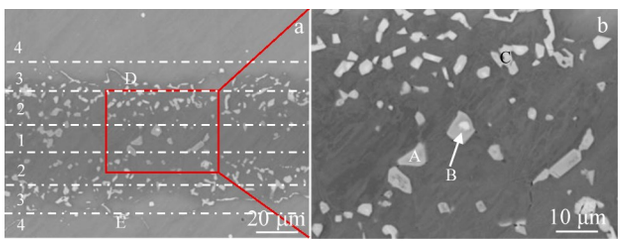

Fig.2 Microstructures of joint with BNi-5 interlayer under conditions of 1130 °C, bonding pressure 10 MPa, and homogenization for 1 h

whereas the matrix in ISZ is γ-Ni. The precipitated phase in DAZ exhibits higher Si and W content than that in BM, with lower contents of Ni, Co, and Mn. Notably, precipitated phase A near the ISZ has a high Cr content. EDS point scanning performed in each region indicates that, except for the white precipitate (E) in BM area, the Si content in other precipitated phases exceeds 11at% (Table 3).

The primary composition element in the joint bonding zone is Ni. And considering that the solubility of Si in Ni is only 8%, the precipitated phases in ASZ, ISZ and DAZ are Si-rich phases. Furthermore, EPMA results reveal higher C content of the precipitated phases in the ASZ, ISZ and DAZ. Since C and Si are chemically similar, they preferentially precipitate at the same location. The Cr content in precipitated phase A is found to be 35.03at%, and EPMA results indicate an enrichment of W. Hence, precipitated phase A is identified as an $M_{23}C_6$ compound rich in Cr and W. Precipitated phase B surrounded by precipitated phase A exhibits a W content of 26.8at%, suggesting that it is M_6C-type compound. Rao et al[27] explained that the Cr content of M_6C-type compounds does not reach the average content in the alloy, leading to the emission of a substantial amount of Cr during the formation of M_6C-type compounds. Consequently, the $M_{23}C_6$ compounds grow along the M_6C lattice direction, ultimately forming a pseudo-eutectic precipitated phase composed of $M_{23}C_6$ and M_6C compounds. The W content in precipitated phases D and E is determined to be 18.6at% and 31.2at% , respectively. Based on previous elemental analyses, it can be inferred that white precipitated phases D and E are both M_6C compounds.

The $M_{23}C_6$ mainly precipitates in ISZ, while M_6C precipitates

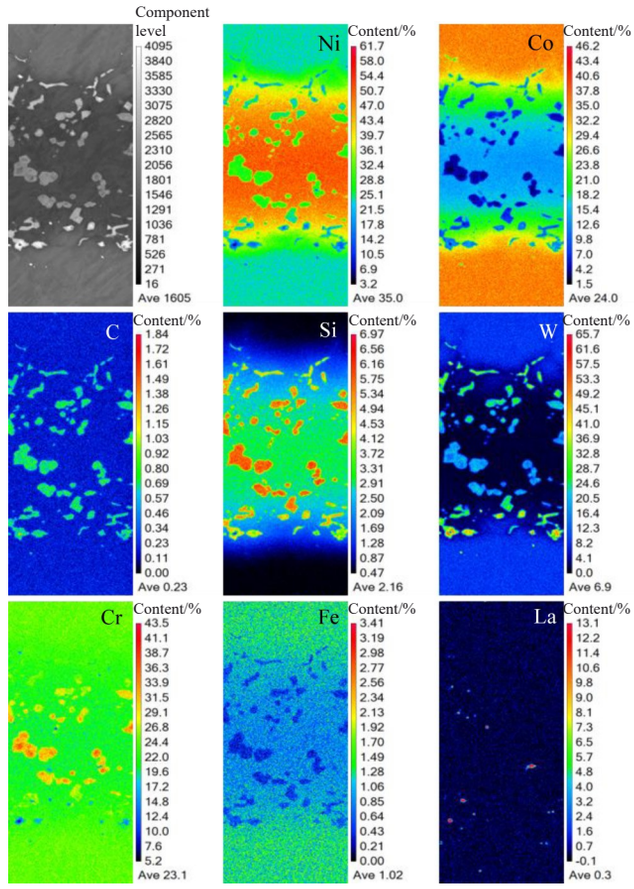

Fig.3 EPMA results of joint with BNi-5 interlayer under conditions of 1130 °C, 10 MPa bonding pressure, and 1 h homogenization

in DAZ, with additional eutectic precipitates (M_6C+$M_{23}C_6$) observed in ISZ. The statistical analysis of the volumes of the two reveals that the size distribution of $M_{23}C_6$ is 3 – 10 μm, while the size of M_6C is mostly 1–3 μm. The interface embedded with the precipitates of $M_{23}C_6$ and M_6C compounds statistically accounts for approximately 26% of the whole interface, obtained by observing the straight interface. In addition, this statistical method is frequently used to calculate the bonded ratio to evaluate the quality of diffusion bonded joints.

Richer information about ISZ is illustrated by transmission electron microscope (TEM) analysis, which shows unique advantages in detecting fine phases composed of different chemical elements. Fig.4b shows that the matrix phase is rich in Co and Ni, which is confirmed by EPMA characterization results. And selected area electron diffraction (SAED) pattern from the [110] zone axis (Fig.4e) reveals a face-centered cubic (fcc) structure (a=0.3596 nm), that is, Ni-rich solid solution and γ phase. In addition, Cr, W, and C are relatively enriched with white phase B, and the composition of the precipitated phase is shown in Table 3. In Fig.4, it is determined that the precipitated phase is the $M_{23}C_6$ compound with a fcc structure (M represents the transition elements Cr, Mo, W, and Re). The interplanar spacing of $(1\bar{1}0)$ fcc is 0.523 nm. High-resolution TEM (HRTEM) image shows lattice fringes with different spacing (Fig. 4c). Filtered inverse fast Fourier transform

Table 3 EDS analysis of points marked in Fig.2 (at%)

Point	C	Si	Cr	Mn	Co	Ni	W
A	0.6	13.9	35.0	2.4	7.1	32.4	8.6
B	0.9	12.1	24.1	1.4	9.1	25.7	26.8
C	0.4	11.0	23.1	2.4	15.9	44.2	1.6
D	0.7	11.5	17.8	1.5	18.5	31.0	18.6
E	0.8	-	22.8	0.8	33.0	11.6	31.2

(IFFT) pattern shows clear details. HRTEM, fast Fourier transform (FFT) spectra, and IFFT images show the interface between the precipitated $M_{23}C_6$ compound (fcc) in zone 1 and the γ matrix (fcc) in zone 2 and zone 3. The joint strength is effectively matched with TEM-EDS analysis results.

3.2 Influence of parameters on joint microstructure

The bonding pressure was maintained at 10 MPa with a bonding time of 1 h. The preset bonding temperature range is 1110 ° C to 1190 ° C, with a 20 ° C interval. The joint morphology at 1130 °C has already been discussed in Section 3.1 and is not repeated here.

As the bonding temperature rises, there is an observable increase in precipitated phases within ISZ. During the isothermal solidification, the ISZ layer forms between the intermediate phase and BM due to the influence of isothermal solidification (Fig. 5). The melting point depressant (MPD) element in the intermediate liquid phase must diffuse into the BM through the ISZ to continuously facilitate the progress of isothermal solidification[23]. In the initial stage, a higher bonding temperature promotes the diffusion of MPD element in the intermediate liquid phase, leading to increased dissolution in the adjacent BM area. This results in a thicker intermediate liquid phase zone, which gradually transforms into ISZ during isothermal solidification. Consequently, MPD elements in the intermediate liquid layer need to diffuse further into the BM to be consumed, but their diffusion rates slow down in the solid phase. This reduction in diffusion rate in the solid phase contributes to a decrease in isothermal solidification rate of the joint. Consequently, a longer bonding time is necessary to eliminate joint eutectic structures that have not completed isothermal solidification. In summary, as the bonding temperature increases, the dissolution of BM intensifies, leading to an increased width of the formed ISZ. This, in turn, results in a decreased isothermal solidification rate, while the aggregation and precipitate formation of MPD elements increase.

As the bonding temperature rises, especially beyond 1130 °C, micro-voids tend to appear in ASZ near the precipitated phase. The eutectic phase in the alloy, having a lower

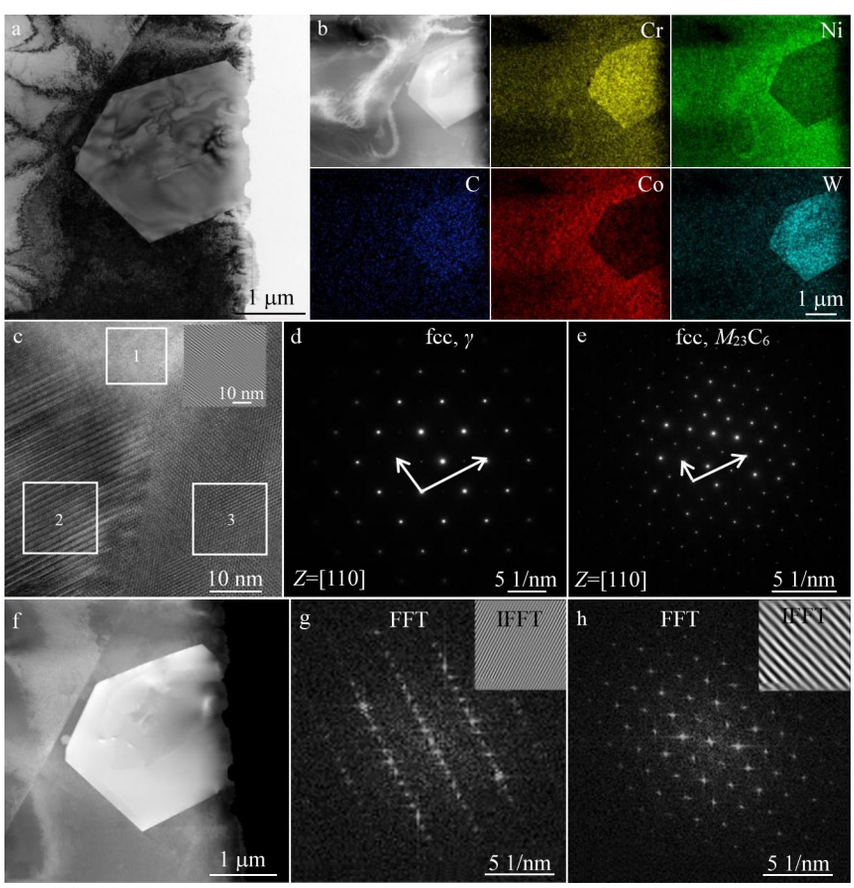

Fig.4 TEM images of local area of ISZ in Fig.2a: (a) bright field image, (b) high-angle annular dark field image and EDS element mappings, and (c) HRTEM image; SEAD patterns of γ phase (d) and $M_{23}C_6$ of zone 1 in Fig.4c (e); HADDF diagram corresponding to Fig.4a (f); FFT and IFFT images corresponding to zone 2 (g) and zone 3 (h) in Fig.4c

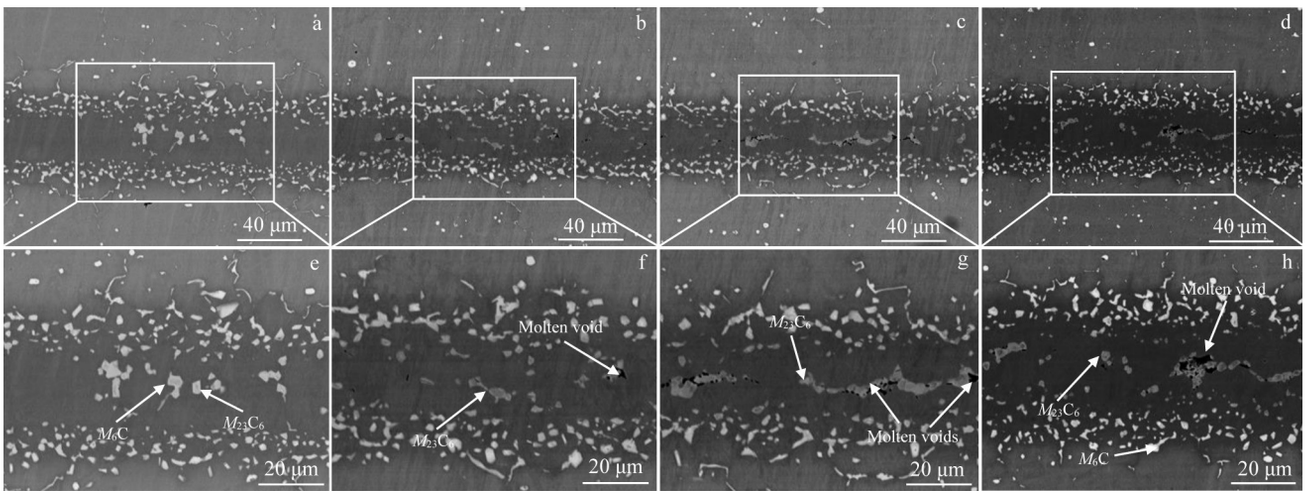

Fig.5 Microstructures of the joint at temperatures of 1110 °C (a, e), 1150 °C (b, f), 1170 °C (c, g), and 1190 °C (d, h)

melting point than the alloy itself, undergoes pre-melting during high-temperature solid solution treatment. This pre-melting occurs below the theoretical melting point of the alloy[30]. Voids form near the pre-melted eutectic phase, serving as potential sources for crack initiation and negatively impacting alloy performance. To address this, an appropriate heat treatment method, such as low-temperature pre-treatment, should be chosen to fully dissolve the eutectic phase. However, if the selected heat treatment temperature does not reach the eutectic temperature of alloy, partial melting may occur due to incomplete dissolution into the BM. With increasing bonding temperature, the likelihood of partial melting rises, leading to an increased number of precipitated phases and voids.

For the precipitated phases in the joint microstructure, EDS spectrum analysis was performed on the joint area at 1150 °C (Fig. 6). No variation in the type of precipitated phases is observed when the bonding temperature is 1130 °C. In ISZ, the precipitated phase is identified as $M_{23}C_6$ compound rich in Cr and W, while in DAZ, the precipitated phase is M_6C compound enriched with W. The increase in temperature does not significantly change the distribution and size of the precipitated phases. The sizes of $M_{23}C_6$ and M_6C are still 3–10 μm and 1–3 μm, respectively.

At 1150 °C with a bonding time of 1 h, the microstructure of the joint is depicted in Fig. 7. Isothermal solidification is accomplished under different bonding pressures of 5, 10, and 15 MPa. Simultaneously, an increase in bonding pressure correlates with the decrease in size of precipitated phase and voids within ASZ, while their quantity rises. As the bonding pressure increases from 5 MPa to 15 MPa, the size of $M_{23}C_6$ decreases from 3–14 μm to 2–6 μm. The diminished size of the precipitated phase may be attributed to increased bonding pressure which facilitates the element diffusion, thereby decreasing the aggregation of elements and resulting in smaller precipitated phases. Conversely, the increased precipitated phase contributes to an increased number of voids dissolved by it. However, the size of the precipitated phase

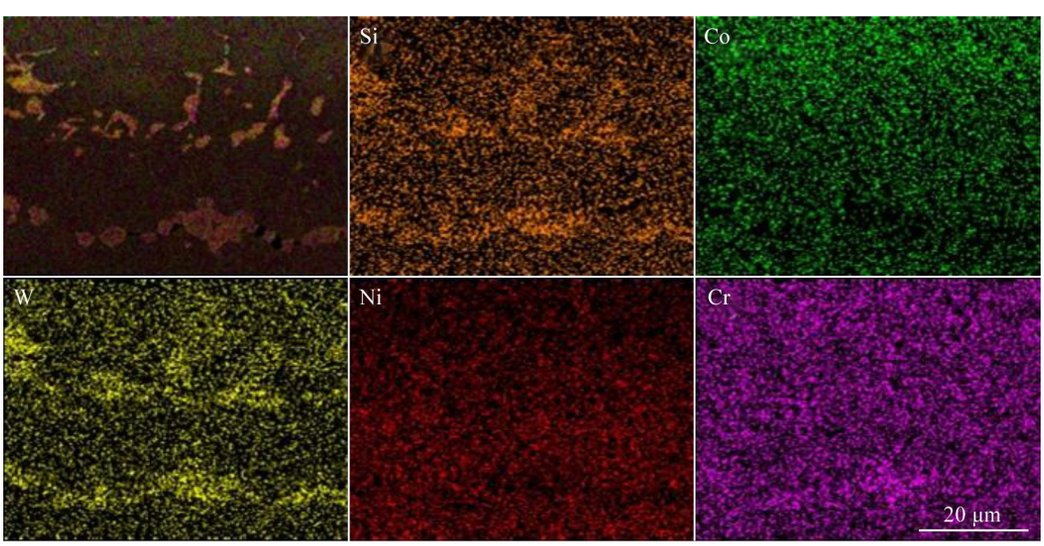

Fig.6 EDS element mappings of joint at bonding temperature of 1150 °C

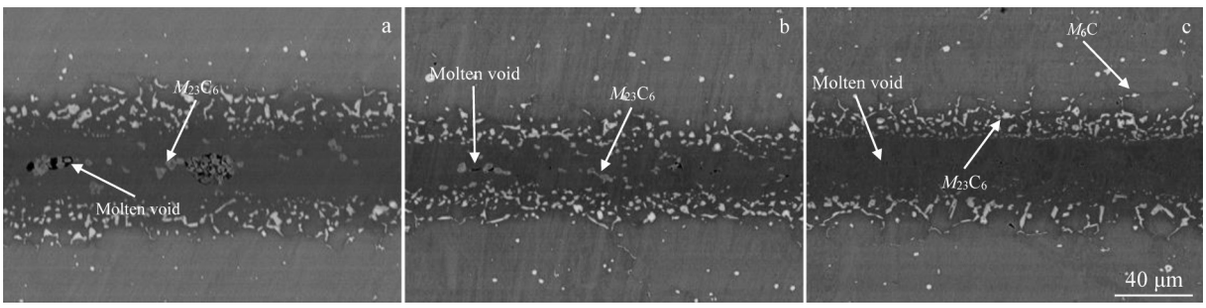

Fig.7 Microstructures of joints at different bonding pressures: (a) 5 MPa; (b) 10 MPa; (c) 15 MPa

constrains the size of the voids, resulting in a decrease in void size as the precipitated phase size decreases.

In Fig. 8a–8c, the orientation and deformation distribution of the joint are depicted by electron backscatter diffraction (EBSD). With an increase in bonding pressure, the interface between BNi-5 and GH5188 gradually diminishes. At bonding pressure of 15 MPa, it becomes challenging to discern the bonding interface, indicating substantial mutual diffusion between BNi-5 and GH5188. The diffusion rate of elements is directly proportional to the applied pressure, and the mutual diffusion coefficient between elements increases with higher pressure. The degree of recrystallization in the joint intensifies with the increase in bonding pressure (Fig. 8d–8f). Moderate pressurization facilitates grain boundary movement and grain rearrangement, promoting the recrystallization process. As bonding pressure rises, the dislocation density at the joint gradually increases, leading to an accumulation of stress. Some grains undergo recrystallization, resulting in a reduction of dislocation density and the release of accumulated stress[35]. Moreover, at bonding pressure of 15 MPa, the deformation of sample has reached the predetermined maximum, and further increasing the bonding pressure might cause excessive deformation, prompting the experiment to refrain from employing a higher bonding pressure.

The microstructure of the joint under different parameters is illustrated in Fig. 9. Joints held for 30 and 60 min both achieved a high degree of isothermal solidification, resembling the joint microstructures obtained under various bonding temperatures in the preceding sections. Precipitated phases are present in ISZ and ASZ, and some of these phases in ASZ are accompanied by voids, as explained earlier. This indicates that precipitated phases and voids persist even after 30 and 60 min of bonding time. The observed persistence suggests that the selected temperature in this study might result in partial melting of the precipitated phase.

For joints with a bonding temperature of 1190 ° C, a bonding pressure of 5 MPa, and no homogeneity time, the microstructure exhibits a large incomplete isothermal solidified eutectic structure in ASZ (Fig. 10). This lager degree of incomplete solidification occurs because isothermal solidification does not fully complete, and the remaining portion of the intermediate liquid phase undergoes cooling and solidification processes. As a result, a brittle eutectic structure with a low melting point formed, adversely affecting the mechanical properties of the joint[25]. To confirm the composition of the ASZ, EDS analysis was conducted

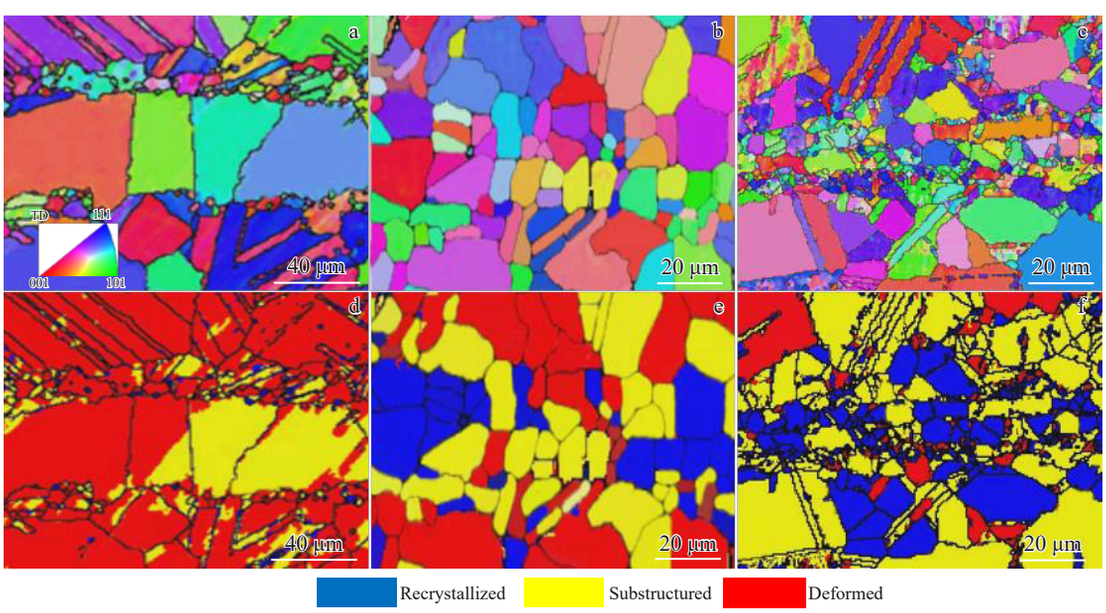

Fig.8 EBSD images of joints at different bonding pressures: (a, d) 5 MPa, (b, e) 10 MPa, (c, f) 15 MPa

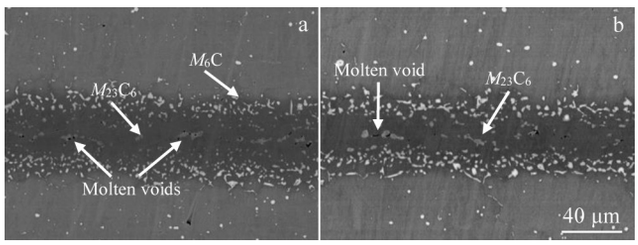

Fig.9 Microstructures of joints with different bonding durations: (a) 30 min; (b) 60 min

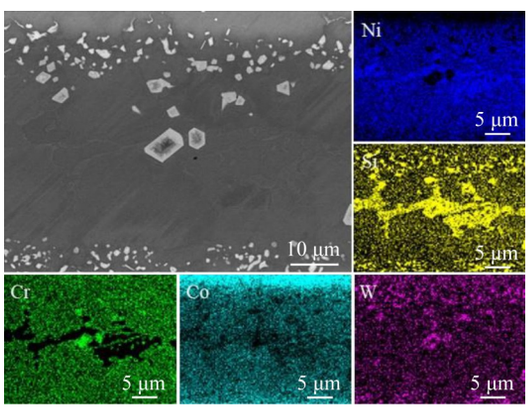

Fig.10 Microstructure and corresponding EDS element mappings of joint at 1190 °C/5 MPa

(Fig. 10). The low-melting-point eutectic structure in ASZ exhibits higher contents of Ni and Si, while the contents of Cr and Co are relatively low, indicating uneven element diffusion. Ni and Si from the BNi-5 brazing material are still abundantly present in the eutectic structure. The elemental distribution of precipitated phase in ISZ and DAZ resembles that of the previously observed precipitated phase. The precipitation phase in ISZ exhibits enrichment of W and Cr, forming an $M_{23}C_6$-type compound. Meanwhile, the precipitated phase in the DAZ is enriched with W, forming an M_6C-type compound.

3.3 Effect of bonding parameters on mechanical properties

Fig. 11 illustrates the tensile shear strength of the joint at different temperatures, maintaining a fixed homogenization

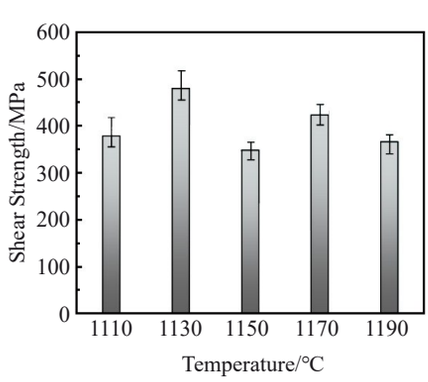

Fig.11 Shear strength of joints at different bonding temperatures

time of 1 h and a bonding pressure of 10 MPa. The tensile shear strength exhibits a trend of increase followed by a decrease. At a bonding temperature of 1130 °C, tensil shear strength reaches their maximum value of 482 MPa, equivalent to 84.6% of that of BM. This peak strength can be attributed to the decrease in size of compounds and voids in ASZ. Compounds exhibit hardness and brittleness, rendering them resistant to plastic deformation under compressive shear loads. This resistance results in stress concentration, which initiates cracks. The stress concentration at the void tips further enhances crack nucleation, leading to crack propagation and coalescence with neighboring cracks, ultimately resulting in joint failure. Reducing the size of compounds generates a pinning effect on dislocations. Additionally, the reduction in void size alters their shape from elliptical to circular, decreasing the stress concentration at the void tips and consequently enhancing joint strength. In addition, the mechanical properties of the joint are closely related to its grain size. As the temperature increases, the grain size at the joint gradually enlarges. Compared to the bonding temperature of 1110 °C, a substantial growth in grain size is observed at 1190 °C, leading to a deterioration in the mechanical properties of the joint (Fig.12). The BNi-5 brazing metal has a melting temperature range of 1080–1135 °C. At bonding temperatures between 1110–1130 °C, small gaps and cracks form at the joint due to the initial melting of BNi-5 solder with poor wettability and fluidity, resulting in underfilling in the edge area. The diffusion of elements in the joint area is insufficient at lower temperatures, unlike at 1130 °C, where the bonding temperature is more suitable for element diffusion (Fig.3 and Fig.6). Consequently, achieving homogenization of the joint composition and obtaining fine microstructures are challenging at lower bonding temperatures, resulting in better mechanical properties.

The microstructures of the joint fracture surfaces in Fig.13a–13b and Fig. 13d–13e exhibit similarities, featuring a rough surface with facet features typical of cleavage fractures. Fig.13 illustrates that the cleavage crack at the fracture origin occurs in the compounds. The plastic deformation capacity of the compounds precipitation at grain boundaries is different from that of the matrix phase. This disparity results in uncoordinated deformation during the shearing process, causing stress concentration. The stress concentration damages the plastic toughness of the grain boundaries, induces cracks at the grain boundaries, and propagates along these boundaries. Ultimately, this process leads to brittle fracture and failure of the joint. Additionally, a significant presence of precipitated phases is observed on the fracture surface. Precipitated phases share similar chemical composition, being rich in C and W, and exhibit M_6C compounds (Fig. 13f). Joints bonded at 1150 °C display a pitted structure in the fracture area, showcasing a ductile-brittle mixed fracture unlike other bonding temperatures (Fig.13c). However, some cracks are apparent on the fracture surfaces, which may account for the lower tensile shear strength of the joint bonded at 1150 °C.

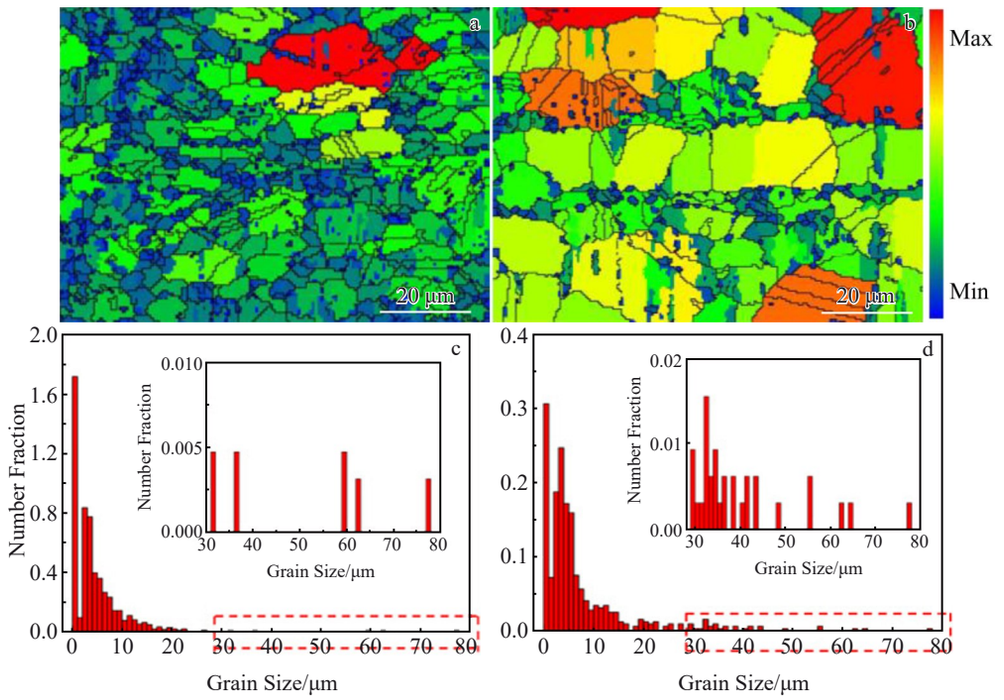

Fig.12 Grain boundary maps (a–b) and grain size distribution (c–d) of joints under different temperatures: (a, c) 1100 °C; (b, d) 1190 °C

Fig. 14 illustrates the shear strength of the joint under various bonding pressures, homogenization for 1 h, and a temperature of 1150 °C. The shear strength of joint is minimal at 5 MPa, and reaches its maximum of 490 MPa at 15 MPa, which represents 86% of that of BM.

The joint bonded at 10 MPa shows a higher number of compounds in ISZ compared to that bonded at 5 MPa. However, the corresponding compounds size in joints bonded at 10 MPa is considerably smaller, rendering it less susceptible to fracture. Furthermore, the smaller compound size serves as a pinning site for dislocations, contributing to enhanced mechanical properties of the alloy. Consequently, the joint bonded at 10 MPa displays slightly greater tensile shear strength compared to that bonded at 5 MPa.

Fig. 15 depicts the fracture surfaces of the joint under different bonding pressures. At 5 MPa, the presence of pits is evident (Fig. 15b). Similar pits are observed on the fracture surfaces of joints bonded at 10 and 15 MPa bonding pressures. However, areas with rough surfaces, pronounced undulations, and stepped features typical of cleavage fracture are also noticeable. The proportion of areas exhibiting cleavage fracture decreases with increasing bonding pressure, while the tendency towards ductile fracture gradually increases. This trend contributes to enhancing the properties.

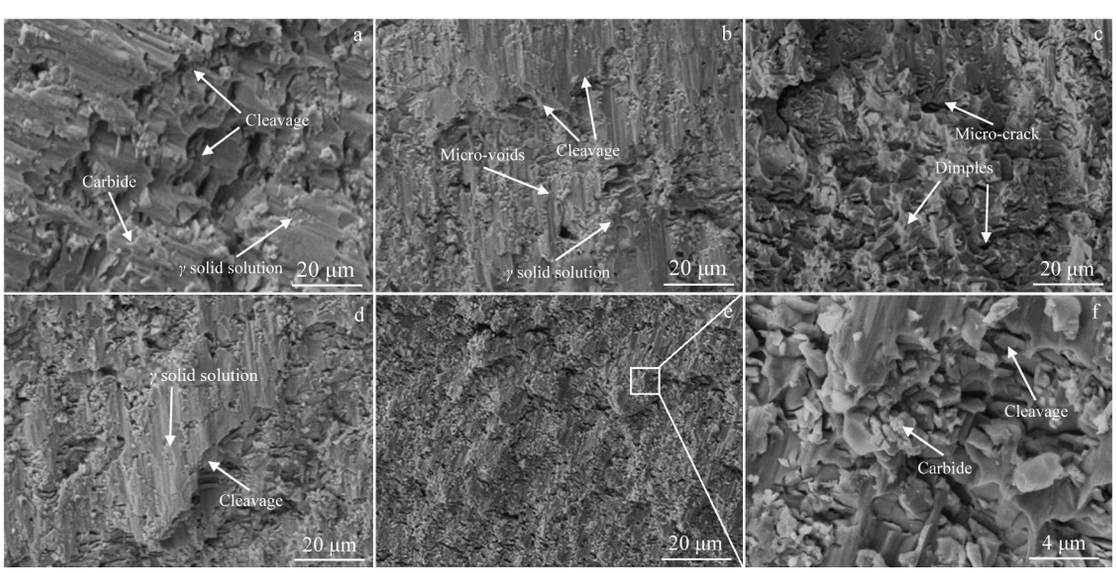

Fig.13 Fracture morphologies of joints at different bonding temperatures: (a) 1110 °C; (b) 1130 °C; (c) 1150 °C; (d) 1170 °C; (e, f) 1190 °C

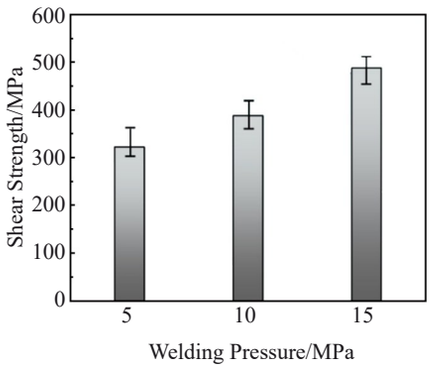

Fig.14 Shear strength of joints under different welding pressures

Tensile-shear tests were performed on joints bonded at 1150 °C/5 MPa for different bonding durations. The results reveal that the joint held for 0.5 h is 355 MPa, while the joint held for 1 h is 321 MPa, indicating minimal difference between them. This observation aligns with the relatively small differences in microstructure between the joints held for 0.5 and 1 h, as evident in the previous section. Based on these findings, it can be concluded that bonding time has a relatively modest effect on the microstructure and mechanical properties when the bonding time ranges from 0.5 h to 1 h. In the absence of homogenization, the joint is susceptible to cracking during the shearing process due to the incomplete ASZ of the joint.

3.4 Formation mechanism of joint

TLP diffusion bonding process of GH5188 alloy can be delineated into four stages, encompassing the melting of intermediate layer, dissolution of BM, isothermal solidification, and composition homogenization. A comprehensive analysis of the microstructure and phase changes of the joint at each of these four stages will be presented in detail (Fig.16).

3.4.1 Melting of intermediate layer

In TLP diffusion bonding process, the selected bonding temperature surpasses the minimum melting point range of the BNi-5 solder (1080–1135 °C), causing the intermediate layer solder to transform into a liquid phase before reaching the set temperature. However, solid-state diffusion takes place in the intermediate layer as it contacts with the BM during the heating process. Si preferentially diffuses into the BM, creating concentration distribution differences of Si within the intermediate layer. This results in higher concentrations in the middle area and lower concentrations on both sides. The actual melting temperature is lower in the middle and higher on both sides. Therefore, the central part of the intermediate layer will undergo melting first upon reaching the liquidus temperature. Subsequently, the liquid phase will propagate to both sides as the temperature continues to rise until complete melting is achieved.

3.4.2 Dissolution of BM

Following the complete melting of the intermediate layer, a liquid layer forms between the two BMs. If the bonding temperature set at this stage is too low, insufficient wetting and spreading of the BNi-5 solder may occur, leading to the presence of numerous unfilled voids. As the liquid intermediate layer spreads entirely, the diffusion of robust element occurs between the liquid phase and the two BMs. Concurrently, the diffusion of Co and W leads to a decrease in melting point of BM near the interface. When the actual melting point falls below the bonding temperature, the BM in this region dissolves, expanding the liquid phase area and facilitating diffusion into the BM. The continuous diffusion between the liquid intermediate layer and BM causes the liquid phase area to expand, and the concentration of MPD element proportionally decreases[28–30].

3.4.3 Isothermal solidification

Following the complete melting of the intermediate layer,

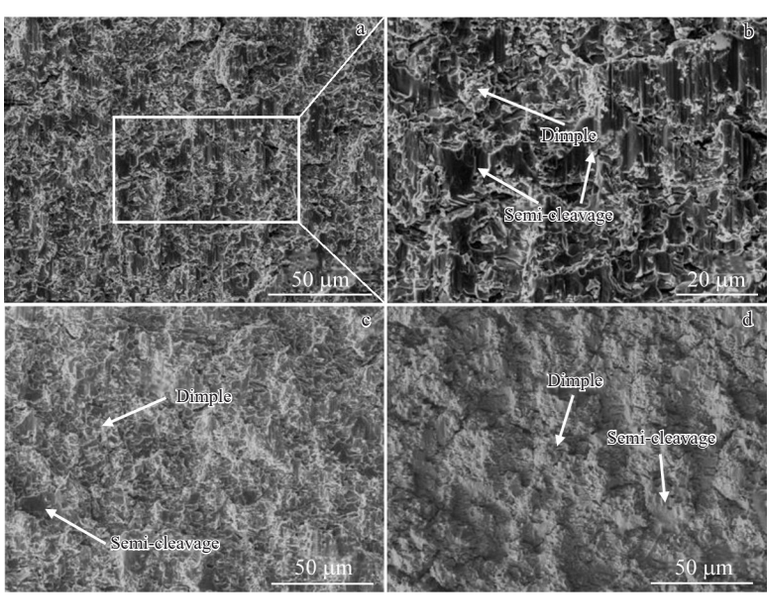

Fig.15 Fracture morphologies of joint under different bonding pressures: (a, b) 5 MPa; (c) 10 MPa; (d) 15 MPa

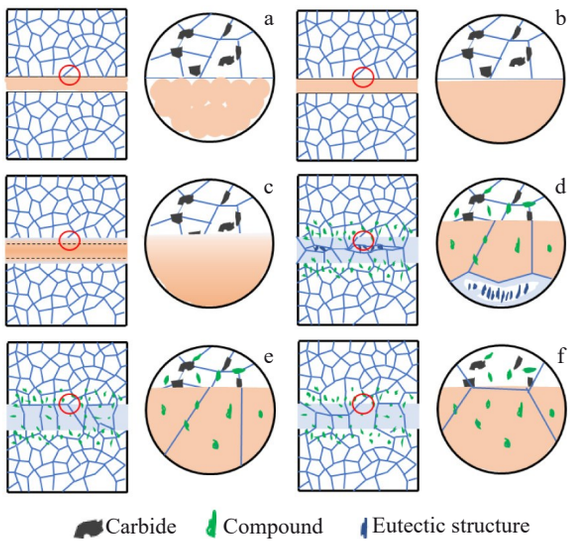

Fig.16 Schematic diagrams of TLP diffusion bonding process of GH5188 alloy: (a) assembly status, (b) melting of the intermediate layer, (c) melting of BM, (d) insufficient isothermal solidification, (e) isothermal solidification, and (f) grain coarsening

three phenomena occur in the joint: Si diffusion to BM, the diffusion of elements in BM into the liquid phase, and the entry of elements into the liquid phase due to BM dissolution. These phenomena determine the liquidus temperature. The impact of these processes depends on the distribution coefficient. Given that the distribution coefficient of Si is less than 1, the liquidus temperature increases as the concentration of Si in the liquid phase decreases[31]. Simultaneously, the enrichment of Cr, Mo, and Ti, with distribution coefficients larger than 1, BM dissolution and diffusion also contribute to an increased liquidus temperature[32–33]. The process of isothermal solidification will take place when the temperature of both is equal. Throughout isothermal solidification, mutual diffusion between the BM and the intermediate layer in the liquid phase stands as the primary driving force for composition changes.

3.4.4 Composition homogenization

Typically, TLP diffusion bonded joints that have undergone isothermal solidification still exhibit notable differences in element concentration compared to the BM[34]. Additionally, the joints may contain numerous compounds in the grain boundaries and grains of DAZ. These compounds frequently serve as sources for crack initiation under load, consequently diminishing the strength of joint[35]. Hence, composition homogenization is often conducted during the bonding stage, and an excessively brief bonding time may impede the completion of this critical phase.

3.5 Strengthening mechanism of joint

Based on the effects of bonding temperature, bonding pressure, and bonding time on joint shear strength, along with the analysis of fracture characteristics, the strengthening mechanism inherent in TLP diffusion bonding of GH5188 alloy with BNi-5 filler metal can be elucidated, as illustrated in Fig.17.

3.5.1 Alloying of joints

Beyond the fundamental element Ni, the BNi-5 soldered intermediate layer also incorporates alloying elements like Cr, Si, and Fe. The solid solubility of C in Ni is relatively significant, approximately 0.6wt%. Ni can solidify compounds and can participate in joint formation, leading to solution strengthening. Simultaneously, MPD element Si induces partial melting of BM into the liquid phase of joint. This mitigates strength loss stemming from the diffusion of the strengthening element to the interlayer during solid-state diffusion bonding. Owing to the rapid diffusion rate of atoms in the liquid phase, a relatively uniform element distribution can be achieved. These elements contribute to alloying process during isothermal solidification of the microstructure. Nano-indentation tests were conducted to shed light on the distribution and evolution of the micro-mechanical properties across the bonding interface. ASZ exhibits the highest hardness value, attributed to the presence of hard and brittle eutectic compounds. In comparison, DAZ shows increased hardness due to the precipitation of Cr, Mo, and W borides. ISZ located at the center of the joint has the lowest hardness value, primarily due to the low content of precipitated phases, which are mainly composed of γ solid solution (Fig.18a). The deformation of ASZ under load is significantly smaller than that of the adjacent ISZ (Fig. 18b). As a result, stress concentration is susceptible to occur in the ASZ, which may lead to cracking of joints from the voids under tensile or shear stress.

3.5.2 Inhibition of grain coarsening in diffusion zone

In TLP diffusion bonding, there is a reduction in volume of certain grain boundary phases due to the diffusion of strengthening elements, and the diffusion rate of Si from the intermediate layer to BM is notably higher than that of other elements. Consequently, compounds can precipitate in both grains and grain boundaries, serving as effective pinning points to prevent grain coarsening in the diffusion zone. The mechanical properties of the joint reveal the emergence of new cleavage planes due to the characteristics of cleavage fracture when passing through compounds. This alteration in the propagation path consumes more energy during the fracture process, contributing to the enhancement of joint strength[36]. In addition, TEM results in Fig.4 demonstrate that the precipitated phase in ISZ is the $M_{23}C_6$ compounds with fcc

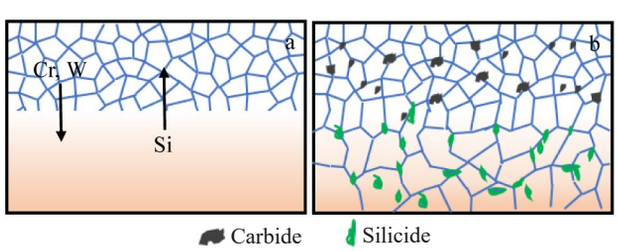

Fig.17 Schematic diagrams of joint strengthening mechanism: (a) joint alloying; (b) inhibition of grain coarsening in diffusion zone

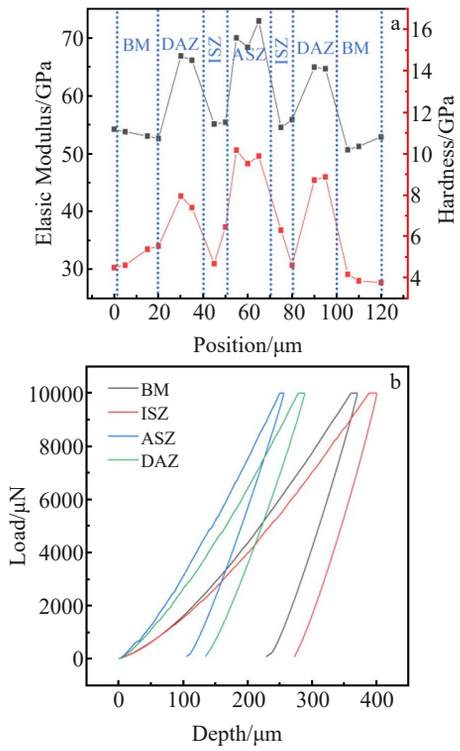

Fig.18 Elastic modulus and hardness distribution over entire bonding interface (a) and typical load-depth diagram (b) of TLP bonding joints at 1190 °C/5 MPa for 60 min

structure (Fig.4e), which can hinder grain boundary migration. Within the pressure setting range, with the increase in pressure, the number of precipitated phases in ISZ increases and the size of precipitated phase decreases. Therefore, the size of the voids caused by the first melting decreases, and the pinning effect is continuously enhanced, which is conducive to the improvement of joint strength.

Under the optimal bonding parameters of 1130 °C, 15 MPa, and 60 min, BM and the interlayer elements achieve significant mutual diffusion, thereby markedly enhancing the alloying degree of the joint. The size of the precipitated phase is notably reduced under these conditions, which significantly increases the pinning effect on dislocations. Concurrently, the size of the voids is reduced, causing the void morphology to transform into a circular shape and decreasing the stress of tip. As a result, these process parameters yield the highest shear strength.

4 Conclusions

1) Solid joints of GH5188 alloy are achieved through TLP bonding utilizing BNi-5 solder. The bonding conditions include temperatures ranging from 1110 ° C to 1190 ° C, pressures between 5 MPa to 15 MPa, and bonding durations of 30 and 60 min. The microstructure of the joint consists of the ASZ, ISZ, DAZ, and BM. The results of TEM and EPMA tests showed that the precipitated phases in BM and DAZ are M_6C, while the primary precipitated phases in ISZ are $M_{23}C_6$.

2) Lower temperatures and higher pressures favor the formation of optimal microstructure in the joint. With an increase in bonding temperature from 1130 ° C to 1190 ° C, there is a gradual increase in precipitated phase within ASZ and ISZ. Simultaneously, elevating the bonding pressure from 5 MPa to 15 MPa leads to an increase in number of precipitated phases in ASZ, accompanied by a decrease in their size. TLP is not sensitive to bonding time, and the change of bonding time in the selected range has no significant effect on the morphology and mechanical properties of the joint.

3) The highest shear strength of 490 MPa, is achieved under the optimal parameters of 1130 °C, 15 MPa, and 30 min. With an increase in bonding pressure from 5 MPa to 15 MPa, tensile shear strength exhibit an upward trend, primarily attributed to the reduction in size of the precipitated phase and the voids in ASZ. Fractography analysis reveals a typical mixed fracture mode, with various dimples and cleavage facets observed along the fracture. Consequently, the small brittle $M_{23}C_6$ phase and voids play a significant role in influencing the mechanical properties of the joints. Nano-indentation tests demonstrate the variations of mechanical properties across the bonding interface, with the ASZ identified as a potential source of cracks.

References

1 Lass E A, Sauza D J, Seidman D N *et al*. *Acta Materialia*[J], 2018, 147: 284

2 Li S W, Liu P K, Chen Y P *et al*. *Materials Characterization*[J], 2023, 203: 113161

3 Ni Haohan, Zeng Qi, Zhang Kai *et al*. *Rare Metal Materials and Engineering*[J], 2023, 52(6): 2302 (in Chinese)

4 Peng Y, Li J L, Li Z X *et al*. *Journal of Manufacturing Processes*[J], 2022, 81: 837

5 Zhang Wei, Chen Zishuai, Dong Ruifeng *et al*. *Rare Metal Materials and Engineering*[J], 2023, 52(9): 3170 (in Chinese)

6 Kong Weijun, Ding Yutian, Wang Xingmao *et al*. *Rare Metal Materials and Engineering*[J], 2023, 52(8): 2859 (in Chinese)

7 Lee W S, Kao H C. *Materials Science and Engineering A*[J], 2014, 594: 292

8 Li P, Sun H T, Wang S *et al*. *Materials Science and Engineering A*[J], 2020, 793: 139843

9 Xiong J T, Yuan L, Zhu Y *et al*. *Journal of Materials Science*[J], 2019, 54: 6552

10 Tabaie S, Rézaï-Aria F, Flipo B C D *et al*. *Materials Characterization*[J], 2021, 171: 110766

11 Liu Yongjun, Long Tianxin, Guo Chengcheng. *Rare Metal Materials and Engineering*[J], 2023, 52(10): 3522 (in Chinese)

12 Yang Zhiming, Chen Zijian, Lin Yongcheng *et al*. *Rare Metal Materials and Engineering*[J], 2023, 52(9): 3147 (in Chinese)

13 Tabaie S, Rézaï-Aria F, Flipo B C D *et al*. *Journal of Materials Science & Technology*[J], 2022, 96: 248

14 Li Z X, Li S W, Xiong J T *et al*. *Journal of Manufacturing Processes*[J], 2022, 84: 1331

15 Wang J, Zhang Y W, Xiong Y L *et al*. *Rare Metal Materials and Engineering*[J], 2022, 51(12): 4446
16 Zhou Fangming, Zhang Fuqiang, Song Feiyuan *et al*. *Rare Metal Materials and Engineering*[J], 2013, 42(9): 1785
17 Tsai C H, Hung H T, Chang F L *et al*. *Journal of Materials Research and Technology*[J], 2022, 19: 2510
18 Wei W, Xiao J C, Wang C F *et al*. *Materials Science and Engineering A*[J], 2022, 831: 142276
19 Pouranvari M, Ekrami A, Kokabi A H. *Materials Science and Engineering A*[J], 2013, 568: 76
20 Wang Chenyang, Xing Fei, Liu Xiangyu *et al*. *Rare Metal Materials and Engineering*[J], 2023, 52(1): 323 (in Chinese)
21 Li S W, Zu Y D, Du Y J *et al*. *Materials Characterization*[J], 2022, 194: 112359
22 Zhao G Y, Jin C B, Zhang R Y *et al*. *Rare Metal Materials and Engineering*[J], 2021, 50(7): 2521
23 Liu J D, Jin T, Zhao N R *et al*. *Materials Characterization*[J], 2011, 62(5): 545
24 Bakhtiari R, Ekrami A. *Materials Characterization*[J], 2012, 66: 38
25 Wikstrom N P, Ojo O A, Chaturvedi M C *et al*. *Materials Science and Engineering A*[J], 2006, 417(1–2): 299
26 Nishimoto K, Saida K, Kim D *et al*. *ISIJ International*[J], 1995, 35(10): 1298
27 Rao K B S, Castelli M G. *Metallurgical and Materials Transactions A*[J], 1997, 28: 347
28 Ghoneim A, Ojo O A. *Materials Characterization*[J], 2011, 62(1): 1
29 Mostafaei M, Abbasi S M. *Journal of Alloys and Compounds*[J], 2015, 648: 1031
30 Xia W S, Zhang X B, Liang Y *et al*. *Journal of Materials Science & Technology*[J], 2020, 44: 76
31 Yuan L, Xiong J T, Ren J *et al*. *Materials Characterization*[J], 2021, 178: 111292
32 Song W Q, Ren J, He P *et al*. *Journal of Manufacturing Processes*[J], 2021, 64: 1476
33 Zhang C, Li M Q, Li H *et al*. *Journal of Manufacturing Processes*[J], 2018, 35: 71
34 Majumdar S, Sengupta P, Kale G B *et al*. *Surface and Coatings Technology*[J], 2006, 200: 3713
35 Liu D H, Chai H R, Yang L *et al*. *Journal of Alloys and Compounds*[J], 2022, 895: 162565
36 Gao Yawei, Dong Jianxin, Yao Zhihao *et al*. *Rare Metal Materials and Engineering*[J], 2017, 46(10): 2922 (in Chinese)

添加BNi-5中间层的GH5188瞬态液相扩散焊连接接头的微观组织和力学性能

郭子龙[1,2]，李昭希[1,2]，郭　伟[1]，刘朋坤[1,2]，李京龙[1]，熊江涛[2]
(1. 西北工业大学 凝固国家重点实验室，陕西 西安 710072)
(2. 西北工业大学 摩擦焊陕西省重点实验室，陕西 西安 710072)

摘　要：采用BNi-5中间层进行GH5188的瞬态液相（TLP）扩散连接。针对GH5188合金及TLP连接机理进行参数选择及优化，研究了接头的组织演变和力学性能。结果表明，相对完整的等温凝固区（ISZ）保证了母材（BM）的可靠连接。在1110 ℃至1190 ℃范围内，较高的连接温度使ISZ增宽，促进了接头成分的均匀化，提高了力学性能。然而，析出相的增加对接头的力学性能产生了不利影响。在1130 ℃时获得了最大的剪切强度，达到482 MPa，占BM强度的84.6%。在5 MPa至15 MPa的压力范围内，非等温凝固区（ASZ）中的析出相和部分熔化产生的空隙均有所增加。相反，它们的尺寸随着连接压力的升高而显著减小，导致合金力学性能呈上升趋势。在15 MPa的连接压力下获得了最大的剪切强度，为490 MPa。接头表现出典型的混合断裂模式，小而脆的$M_{23}C_6$相和空隙显著影响力学性能。纳米压痕测试表明ASZ是裂纹的潜在来源。

关键词：瞬态液相扩散焊；GH5188钴基高温合金；BNi-5中间层；组织演变；力学性能

作者简介：郭子龙，男，2001年生，硕士生，西北工业大学凝固国家重点实验室，陕西 西安 710072，E-mail：guozilong@mail.nwpu.edu.cn；李昭希，男，1997年生，博士生，西北工业大学凝固国家重点实验室，陕西 西安 710072，E-mail：zxli@mail.nwpu.edu.cn